MISSOURI
S&T

Missouri University of Science and Technology

Scholars' Mine

International Specialty Conference on Cold-Formed Steel Structures

Wei-Wen Yu International Specialty Conference on Cold-Formed Steel Structures 2018

Nov 7th, 12:00 AM - Nov 8th, 12:00 AM

A Finite Element Study of Corrugated Steel Deck Subjected to Concentrated Loads

Vitaliy V. Degtyarev

Follow this and additional works at: https://scholarsmine.mst.edu/isccss

Part of the Structural Engineering Commons

A Finite Element Study of Corrugated Steel Deck Subjected to Concentrated Loads

Vitaliy V. Degtyarev[1]

Abstract

An extensive parametric study was initiated to get a better understanding of steel deck behavior under concentrated loads and to develop design recommendations for a wide range of deck profiles. This paper presents first results from the study related to 1.5-in. deep roof decks of types B and F. The study was performed on non-linear finite element models of deck validated against available test data. Deck gage, span length, span condition, concentrated load locations along and across the deck span were varied in the study. The observed deck behavior under concentrated loads, as well as the effects of the studied parameters on the effective distribution widths governed by the deck strength and stiffness, was presented and discussed. Design equations for predicting the effective distribution width for the studied deck profiles were presented.

Introduction

In modern construction, mechanical, electrical and plumbing (MEP) components are often suspended directly from corrugated steel deck and induce heavy concentrated loads to it (Fig. 1). Design of the deck for concentrated loads requires knowledge of load distribution across the deck panels, published information on which is very limited.

Johansson (1986) proposed a simple analytical model for computing bending moments and deflections of single- and double-span trapezoidal profiles under a point load applied at the mid-span of the deck. Deck deflections and strains predicted by the proposed model were compared with those obtained experimentally for nine different deck types; and a fairly good agreement was reported. However, it was pointed out that the model calibration against the test data might be required. The laboratory tests showed that nearly only the loaded

[1] Design and Research Engineer, New Millennium Building Systems, LLC, Columbia, SC, USA

flute and two adjacent flutes of the deck are active in carrying the concentrated load applied at the deck mid-span.

Fig. 1. MEP components suspended from steel roof deck

The behavior of simply supported 1.5-in. (38 mm) deep steel deck of type B with plywood overlay was studied experimentally at the University of Missouri-Rolla (Bahr 2006). Several parameters were varied in the study, such as: deck steel thickness, plywood thickness, the load bearing plate size, the point load location along the deck span, as well as attachments of the plywood to the deck and the deck to the supports. Design recommendations for predicting transverse distribution width for the studied deck-plywood assemblies were developed.

Šorf and Jandera (2017) reported results of experimental and finite element (FE) studies of trapezoidal deep decks with hanging loads applied to the deck webs. Formulas for predicting hanging load distribution between the loaded and adjacent deck flutes were proposed. It was concluded that the developed formulas provided good and safe results for the load located at the mid-span. The formulas gave more conservative results for the load located at L/7 from the support. It was also concluded that FE model can predict the deck behavior under concentrated loads reasonably well.

A user note in ANSI/SDI RD-2017 gives the following guidelines for the transverse distribution width of a concentrated load in the middle half of the span

of a 1.5-in. (38 mm) deep deck: the load footprint width plus 12 in. (300 mm) but not less than 18 in. (460 mm) distribution width. The standard references SDI RDDM1 (2012) for more information. SDI RDDM1 presents equations for determining the transverse distribution width for the 1.5-in. (38 mm) deep decks, which are functions of concentrated load location along the deck span and the load footprint width. The SDI RDDM1 equations were developed based on the University of Missouri-Rolla study (Bahr 2006), where the concatenated load was applied through plywood overlay. The applicability of the equations to the loads applied directly to the deck is questionable.

Several deck manufacturers have ICC-ES evaluation reports for wedge hangers installed into re-entrant steel deck profiles. The evaluation reports contain allowable hanging loads for different deck types, which are based on physical testing in accordance with ICC-ES AC379.

The presented literature review shows that research on this subject is scarce; and design recommendations are limited. To get a better understanding of the steel deck behavior under concentrated loads and to develop design recommendations for a wide range of steel deck profiles, an extensive numerical parametric study was initiated. This paper presents first results from the study related to 1.5-in. (38 mm) deep roof deck profiles of types B and F. The study was performed on non-linear FE models of steel deck validated against available test data. In addition to the deck type, the following parameters were varied in the study: deck gage, deck span length, deck span condition and concentrated load locations along and across the deck span.

Finite element model

Nonlinear three-dimensional FE models of different steel deck profiles were developed in ANSYS using 4-node structural shell elements SHELL181 with the elastic-perfectly plastic bilinear isotropic hardening material behavior (BISO) using von Mises plasticity. An elastic modulus of 29500 ksi (2.03×10^5 MPa) and a Poisson's ratio of 0.3 were used for the deck. The models were discretized with quadrilateral meshes. The mesh density was selected based on convergence studies. The deck boundary conditions represented those in real structures. Vertical translations of all bottom flange nodes at the locations corresponding to the deck supports were restrained. In addition, longitudinal and transverse translations of one node of each bottom flute were restrained at the deck support locations to model deck attachments to supports.

The elastic buckling analysis was performed to obtain the elastic shear buckling mode of the deck, which was used for modeling the initial geometric imperfection

of the deck. The initial geometric imperfection magnitudes of 0.15t, 0.64t and b_{tf}/150 recommended by Camotim and Silvestre (2004), Schafer and Pekoz (1998), and Keerthan and Mahendran (2011), respectively, were considered. The studied imperfection magnitudes showed no significant difference in the behavior and strength of the deck under concentrated loads. Therefore, the initial geometric imperfection magnitude of 0.64t was used in the study. The deck models were loaded by imposed vertical displacements applied in small increments to the node coinciding with the concentrated load location.

The developed models were validated against allowable concentrated loads for wedge hangers published in ICC-ES evaluation report ESR-3477 (2017). The ESR-3477 allowable loads were obtained from physical tests by dividing the maximum load supported by the deck by a safety factor of five. Therefore, the allowable concentrated loads from the report were multiplied by five and compared with the maximum load obtained from the FE analyses. The comparison results presented in Table 1 show that the developed models predicted the test results reasonably well.

Table 1. Model validation results

Deck Type	Gage	L, in. (mm)	P_a, lbs (N)	P_n, lbs (N)	P_{FEA}, lbs (N)	P_{FEA}/P_n
	20	31 (787)	171 (761)	855 (3803)	1022 (4546)	1.20
		144 (3658)	51 (227)	255 (1134)	206 (916)	0.81
Versa-Dek S Acoustical	18	31 (787)	266 (1183)	1330 (5916)	1471 (6543)	1.11
		165(4191)	94 (418)	470 (2091)	580 (2580)	1.23
	16	31 (787)	334 (1486)	1670 (7429)	1972 (8772)	1.18
		189 (4801)	153 (681)	765 (3403)	764 (3398)	1.00
	20	31 (787)	186 (827)	930 (4137)	1010 (4493)	1.09
		228 (5791)	53 (236)	265 (1179)	222 (988)	0.84
Versa-Dek 3.5 LS Acoustical	18	31 (787)	360 (1601)	1800 (8007)	1853 (8243)	1.03
		240 (6096)	121 (538)	605 (2691)	665 (2958)	1.10
	16	31 (787)	521 (2318)	2605 (11588)	2846 (12660)	1.09
		261 (6629)	225 (1001)	1125 (5004)	1094 (4866)	0.97
					MIN	0.81
					MAX	1.23
					MEAN	1.05
					COV	0.126

Parametric study

The parametric study described in this paper was performed on FE models of 1.5-in. (38 mm) deep roof decks of types B and F shown in Fig. 2. A preliminary study showed that the profile corner radii had negligible effects on the deck strength and behavior under consternated loads. Therefore, the corner radii were not included into the models.
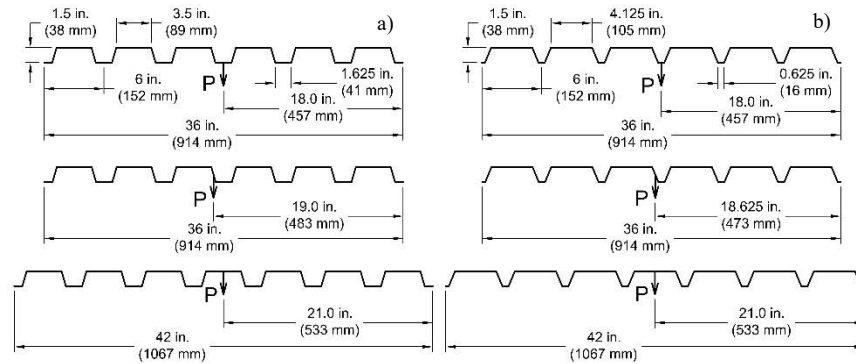
Fig. 2. Studied a) type B and b) type F decks with point loads at different locations across the deck span (bottom flange, web and top flange)

The following parameters were varied in the models:
- deck steel thickness: 22GA (0.0295 in. (0.75 mm)); 18GA (0.0474 in. (1.20 mm)); and 16GA (0.0598 in. (1.52 mm));
- deck span condition: single and triple;
- deck span: 3 ft (914 mm), 6 ft (1829 mm), and 9 ft (2743 mm);
- concentrated load location along deck span:
    o $L/8$, $L/4$, $3L/8$, and $L/2$ for single spans;
    o $L/8$, $L/4$, $3L/8$, $L/2$, $5L/8$, $3L/4$, $7L/8$, $9L/8$, $5L/4$, $11L/8$ and $3L/2$ for triple spans;
- concentrated load location across deck span: at the bottom flange, at the top flange and at the web.

Concentrated loads were applied at the center of the panel width as shown in Fig. 2. The FE models were as described in the previous section with the yield stress of 40 ksi (276 MPa). The top flanges and webs of the models were discretized with eight and four elements, respectively. The bottom flanges of the B and F decks were meshed with four and two elements, respectively. The length of the shell elements along the deck span were 1.5 in. (38 mm) in all models. The analyses were performed as described in the previous section.

Behavior of steel deck under concentrated loads

Figure 3 shows typical load-deflection curves for a 0.0474-in. (1.2 mm) thick B deck of different spans subjected to concentrated loads applied at different locations along and across the deck span. The typical structural response of the deck is characterized by an initial elastic phase, followed by a non-linear plastic

phase, and finally by a hardening phase due to the membrane action. As known from the large-deflection theory of thin plates (Ventsel and Krauthammer 2001), the membrane action (that is, tension of the plate middle surface) becomes comparable with the bending action when the plate deflection reaches the order of the plate thickness. Further increase in the plate deflection makes the membrane action predominant. The structural response of the deck presented in Fig. 3, shows that the membrane action in the corrugated steel deck becomes predominant when the deck deflections were in the order of the deck height.
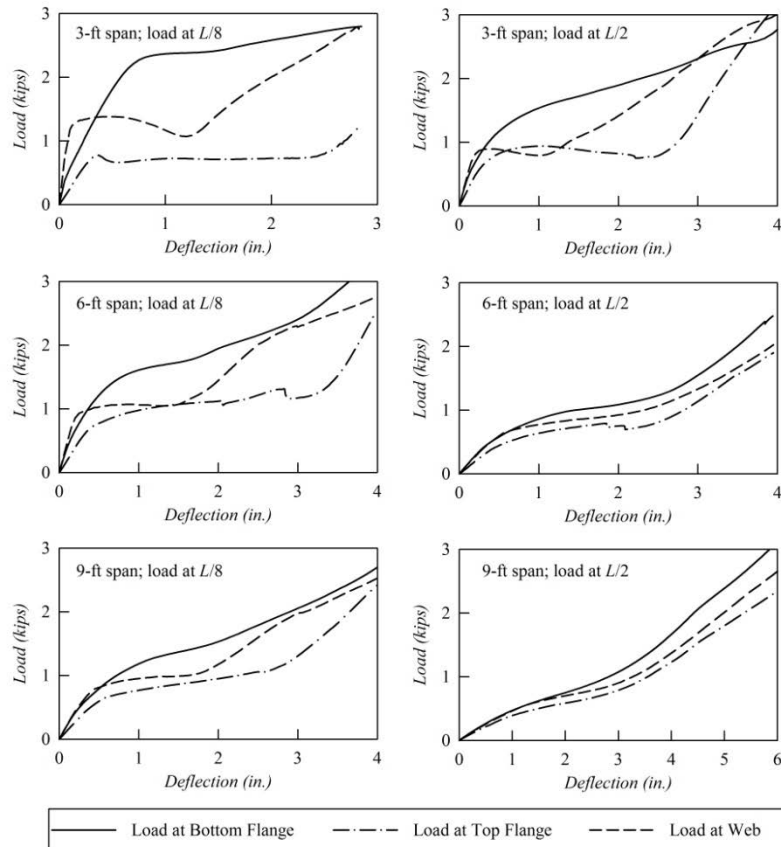
Fig. 3. Load-deflection curves for type B deck

As can be seen from Fig. 3, steel deck can support very heavy concentrated loads when the membrane action occurs. However, to allow for the membrane action,

the membrane forces shall be considered in the design of the deck connections to the supporting members, as well as in the design of the supporting members, which is not typically done in the engineering practice. Therefore, in this study, the maximum concentrated load that can be supported by the deck was limited to the load at the hardening phase onset. Figure 3 also shows that the structural response of the deck depended on the location of the point load along and across the deck span, as well as on the deck span length.

Effective transverse distribution width of a concentrated load

The effective transverse distribution widths for each analyzed model were determined using maximum concentrated loads from the FE analyses and section properties of the deck. The effective distribution widths governed by deck strength and stiffness were considered. The positive moment capacity of the deck controlled the maximum load applied to the deck. Therefore, the effective width governed by the deck strength was determined using Eq. (1) based on the deck positive moment capacity. The effective width governed by the deck stiffness was determined from Eq. (2) using deck deflection under the concentrated load corresponding to 60% of the maximum load.

$$b_e(M_p) = M_P/(M_n - M_w) \tag{1}$$
$$b_e(\Delta) = \Delta_t(0.6P_{max})/[\Delta_{FEA}(0.6P_{max}) - \Delta_w] \tag{2}$$

Effects of parameters

Figures 4 and 5 show plots of the effective transverse distribution width versus the relative point load location along the deck span for single and triple span decks, respectively. For all considered cases, the effective distribution width increased when the point load location approached the mid-span of the deck. Concentrated loads distributed over wider widths for the decks with longer spans and thicker base steel. These results were expected based on the available information about concentrated load distribution in composite deck slabs (ANSI/SDI C-2017).

Figures 4 and 5 show that the load location across the deck span significantly affected the effective distribution width. Wider distribution widths were obtained for the load applied at the deck bottom flange, followed by the load applied at the deck web. Smaller distribution widths were obtained for the load applied at the deck top flange.
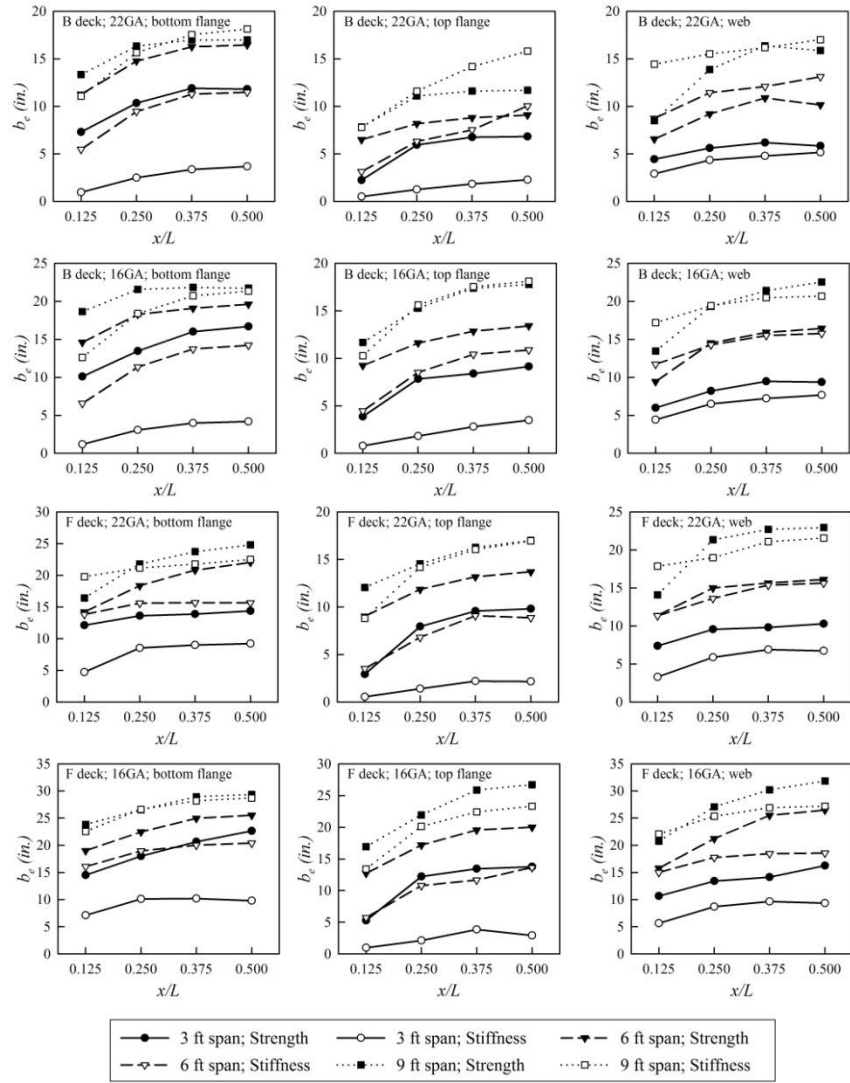
Fig. 4. Effect of point load location along deck span on effective distribution width for single span deck
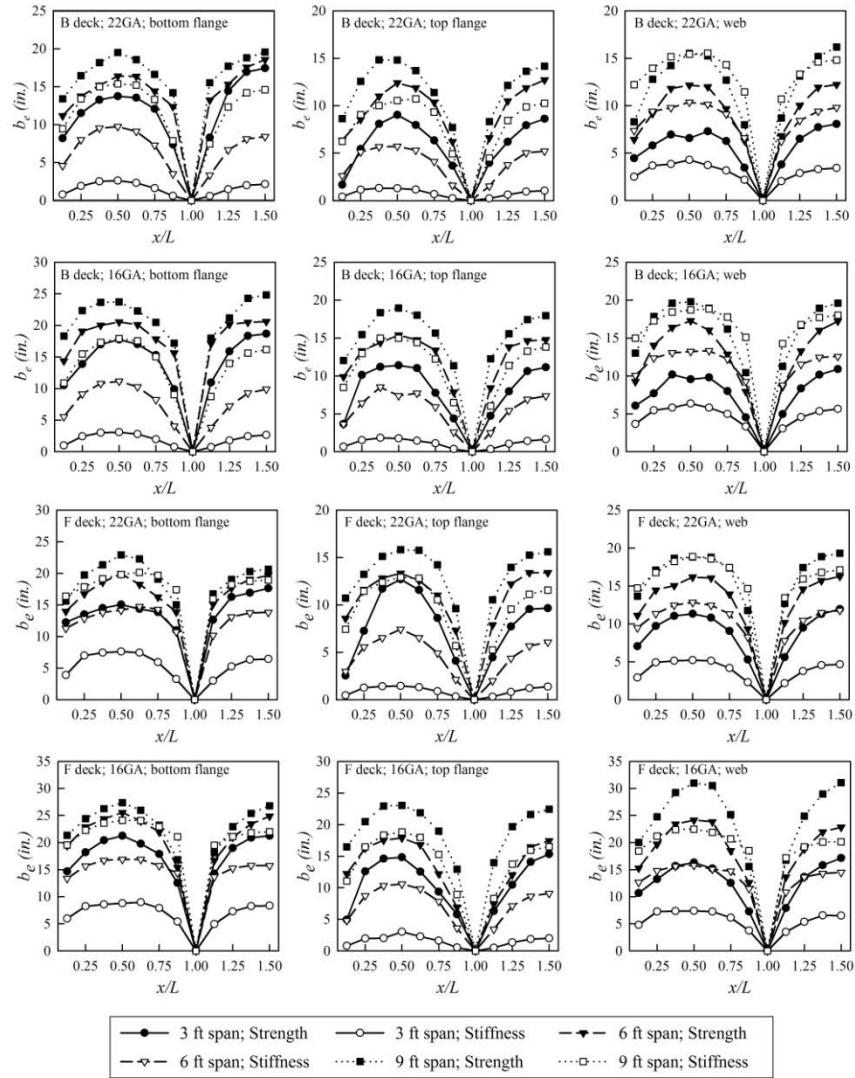
Fig. 5. Effect of point load location along deck span on effective distribution width for triple span deck

Two factors are deemed to play key roles in the effective width reduction for the load at the deck top flange: the effect of the web crippling and moment interaction, and the local bending of the deck top flange. When a concentrated load is applied at the top flange, significant local compression stresses are induced in the deck webs, especially when the load is located near the deck support, which may result in significant moment and web crippling interaction. The deck moment capacity and the effective distribution width reduce as a result of the interaction. The top flanges of the considered profiles were wider than the bottom flanges. A heavy concentrated load applied to the deck top flange caused the top flange local bending, which resulted in the section depth reduction at the point load location and contributed to the local buckling strength reduction of the compressed top flange of the deck.

The distribution widths for the loads applied at the bottom flanges were greater than those for the loads applied at the web because the loads were distributed to two deck webs through relatively narrow deck bottom flanges. The rigid (for in-plane bending) deck webs transferred the concentrated loads further across the deck panels. When a load was applied at the web, it was distributed through the relatively wide and flexible top flange of the deck, whose bending stiffness and the ability to distribute concentrated loads across the deck panel are limited.

The effective distribution widths of the concentrated loads applied to type F deck were generally greater than those for type B deck. It was also found that the effective transverse distribution widths governed by strength may differ significantly from the effective distribution widths governed by stiffness. The effective distribution widths governed by stiffness were considerably smaller than the effective widths governed by strength in many cases.

Design equations for predicting effective transverse distribution width

Shapes of the curves shown in Figs. 4 and 5 imply that the obtained effective distribution widths could be described by a parabolic function of the load location along the deck span represented by Eq. (3). To capture the effects of deck thickness and span length observed in the study, the coefficient k in Eq. (3) was expressed through those parameters by Eq. (4).

$$b_e = k(1 - x/L)\,x/L \tag{3}$$
$$k = (k_{t1}t + k_{t2})(k_{L1}L + k_{L2}), \tag{4}$$

where $b_e \geq 0.5$ in. (12.7 mm) for the effective width governed by stiffness.

The coefficients k_{t1}, k_{t2}, k_{L1} and k_{L2} were determined using a nonlinear regression analysis of the FE simulation results. Different deck types, different point load locations across the deck span and different span conditions were

considered separately. Values of the coefficients obtained from the regression analysis are given in Table 2. Comparisons of the effective transverse distribution widths from the FE simulations and calculated using Eq. (3) are shown in Fig. 6 a) and b) for the effective widths governed by strength and stiffness, respectively. The comparisons show that Eq. (3) can predict the effective widths reasonably well, but it tends to underestimate the effective distribution widths of the concentrated loads located near the supports.

Table 2. Coefficient values in Eq. (4)

Deck Type	Span Condition[1]	Load Location[2]	Governed by Strength				Governed by Stiffness			
			k_{t1}	k_{t2}	k_{L1}	k_{L2}	k_{t1}	k_{t2}	k_{L1}	k_{L2}
B	S	B	24.16	1.88	1.64	16.68	19.49	2.66	3.33	-5.50
B	S	T	34.65	1.37	2.01	5.50	37.23	3.21	2.05	-4.20
B	S	W	38.55	1.55	2.46	3.51	29.68	2.57	2.56	-0.02
B	T-E	B	41.43	3.45	0.94	10.02	14.22	2.53	3.17	-6.06
B	T-I	B	20.54	2.54	1.22	18.54	10.43	2.35	3.30	-6.77
B	T-E	T	33.54	2.20	1.39	7.02	28.90	1.36	3.11	-7.43
B	T-I	T	19.51	1.53	2.06	11.25	28.20	1.54	2.68	-6.74
B	T-E	W	28.27	1.61	2.35	6.13	25.61	2.15	2.86	-1.56
B	T-I	W	23.35	1.76	2.22	7.74	31.25	2.45	2.41	-1.90
F	S	B	31.23	2.65	1.66	15.47	26.76	2.52	3.36	1.95
F	S	T	36.61	1.13	2.9	8.81	41.9	1.79	3.42	-7.53
F	S	W	46.69	2.03	2.48	6.9	29.79	2.34	3.46	-0.14
F	T-E	B	27.26	2.23	1.36	19.56	21.84	2.59	3.12	1.04
F	T-I	B	23.18	2.69	0.76	21.22	18.63	2.52	3.21	0.5
F	T-E	T	35.58	1.92	1.67	9.11	35.11	1.22	3.56	-8.1
F	T-I	T	32.6	2.06	1.45	10.05	29.23	1.03	3.78	-9.1
F	T-E	W	57.75	1.88	1.92	7.42	25.24	2.42	3.16	-1.31
F	T-I	W	32.23	1.28	3.04	12.98	22.6	2.23	3.24	-1.91

Notes: 1) S = single span; T-E = triple exterior span; T-I = triple interior span.
    2) B = bottom flange; T = top flange; W = web.

The effective transverse distribution width can be better approximated by a quartic function described by Eqs. (5)-(8) with the coefficients as shown in Table 3. Comparisons of the effective transverse distribution widths from the FE simulations with those predicted by Eqs. (5)-(8) are shown in Fig. 6 c) and d). The comparisons demonstrate that Eqs. (5)-(8) provide better approximations of the effective transverse distribution widths from the FE simulations when compared with Eqs. (3) and (4).

$$b_e = k_a(x/L)^4 + k_b(x/L)^3 + k_c(x/L)^2 - (k_a + k_b + k_c)(x/L) \tag{5}$$
$$k_a = (k_{ta1}t + k_{ta2})(k_{La1}L + k_{La2}) \tag{6}$$
$$k_b = (k_{tb1}t + k_{tb2})(k_{Lb1}L + k_{Lb2}) \tag{7}$$
$$k_c = (k_{tc1}t + k_{tc2})(k_{Lc1}L + k_{Lc2}) \tag{8}$$

where $b_e \geq 0.5$ in. (12.7 mm) for the effective width governed by stiffness.

Table 3. Coefficient values in Eqs. (6)-(8)

Deck Type	Span Condition[1]	Load Location[2]	k_{t1a}	k_{t2a}	k_{L1a}	k_{L2a}	k_{t1b}	k_{t2b}	k_{L1b}	k_{L2b}	k_{t1c}	k_{t2c}	k_{L1c}	k_{L2c}
						Governed by Strength								
B	S	B	92.54	4.10	-6.36	0.37	-129.97	-5.82	-8.99	0.51	100.15	4.97	-7.24	-4.84
B	S	T	-61.77	-4.56	5.71	-15.07	-85.59	-6.34	-8.22	21.71	-79.22	-5.14	6.52	-13.55
B	S	W	-37.13	-2.55	2.69	17.88	-47.88	-3.42	-4.06	-27.17	-49.63	-3.15	4.05	19.27
B	T-E	B	61.25	4.46	-5.60	-5.06	-96.81	-6.16	-7.84	-6.13	85.02	4.86	-6.51	-9.73
B	T-I	B	19.87	7.99	-5.40	-3.18	-25.25	-11.01	-7.91	-4.60	23.42	7.87	-7.02	-10.98
B	T-E	T	-123.77	-3.80	3.72	-15.28	171.62	6.42	5.03	-20.73	-98.96	-5.40	5.03	-16.09
B	T-I	T	-74.41	-4.30	4.36	-11.44	101.47	6.20	6.20	-16.26	-70.57	-4.87	5.66	-9.84
B	T-E	W	47.33	1.02	-4.54	-0.97	-90.08	-1.22	-5.73	-0.65	-91.22	-1.38	4.83	3.12
B	T-I	W	-80.81	-3.60	2.98	-6.97	110.74	4.91	4.36	-10.20	-72.21	-3.84	4.58	-5.60
F	S	B	125.62	2.07	-5.78	-16.67	-179.97	-2.92	-8.12	-23.22	141.64	3.13	-6.45	-22.78
F	S	T	-105.65	-5.15	5.97	-20.59	-130.57	-6.15	-9.83	33.89	-111.04	-4.55	8.35	-23.29
F	S	W	-22.89	-4.98	3.79	26.06	-31.74	-7.07	-5.33	-37.04	-42.78	-6.28	4.58	26.88
F	T-E	B	44.41	4.51	-2.63	-37.69	72.18	6.41	3.76	50.75	75.67	5.71	-3.13	-40.01
F	T-I	B	-18.30	6.50	-2.65	-52.24	-26.00	9.23	3.73	73.57	-12.89	8.52	-2.66	-55.35
F	T-E	T	-12.18	-6.34	6.91	-27.36	46.78	10.99	7.47	-28.98	-75.15	-7.15	6.41	-19.00
F	T-I	T	-60.89	-5.30	4.46	-13.80	89.88	7.22	6.35	-19.66	-73.93	-5.11	5.74	-11.68
F	T-E	W	-17.17	5.95	-5.58	-2.27	20.86	-8.93	-7.22	-4.68	-13.89	-6.20	6.37	10.10
F	T-I	W	-11.90	-6.25	4.07	-0.89	17.28	8.01	6.25	-1.17	-37.82	-5.73	5.56	4.20
						Governed by Stiffness								
B	S	B	-42.68	-5.76	5.32	-23.28	-60.77	-7.96	-7.64	33.43	-72.17	-9.31	4.89	-18.83
B	S	T	-164.74	-7.57	1.65	-8.76	254.74	13.02	2.02	-10.73	-125.8	-8.79	2.77	-12.48
B	S	W	-84.85	-4.21	8.29	-18.38	-107.16	-5.21	-13.27	29.43	-105.08	-5.45	8.93	-17.65
B	T-E	B	24.33	4.86	-4.59	21.32	-38.63	-7.19	-6.22	28.20	-48.40	-8.37	4.22	-16.13
B	T-I	B	-71.32	-10.2	1.56	-7.88	107.51	16.26	1.98	-10.02	-51.74	-9.71	2.88	-12.25
B	T-E	T	6.33	5.00	-2.44	12.52	-31.59	-6.93	-3.24	15.63	-82.38	-6.18	2.62	-9.87
B	T-I	T	-33.20	-1.81	1.35	-13.50	-54.00	-2.84	-1.69	16.93	-72.52	-4.15	1.74	-9.86
B	T-E	W	-109.49	-2.69	7.18	-17.22	-130.84	-3.24	-11.87	27.92	-124.9	-3.85	7.85	-16.17
B	T-I	W	-112.55	-1.57	7.53	-19.37	-144.18	-1.97	-11.81	30.44	-152.71	-2.95	7.13	-16.75
F	S	B	-11.09	-7.96	9.09	-8.65	-14.24	-10.27	-14.10	13.42	-21.06	-8.87	10.79	-8.31
F	S	T	-102.98	-2.51	4.57	-20.68	-152.48	-3.95	-6.04	27.32	-185.98	-6.10	3.61	-14.33
F	S	W	-105.36	-4.62	8.55	-17.11	-132.53	-5.78	-13.64	27.30	-126.58	-5.99	9.41	-16.72
F	T-E	B	-69.31	-7.41	7.44	-14.10	-81.74	-8.40	-12.71	23.34	-70.75	-7.05	9.91	-15.04
F	T-I	B	-97.38	-4.81	9.13	-21.03	-120.75	-5.94	-14.75	34.00	-108.08	-6.02	10.36	-21.46
F	T-E	T	97.10	1.95	-3.58	17.97	-135.63	-2.81	-5.27	25.68	-172.41	-4.47	3.28	-13.38
F	T-I	T	-141.25	-3.46	1.36	-7.98	237.12	6.20	1.58	-9.30	-130.82	-4.26	2.47	-11.51
F	T-E	W	-109.61	-3.40	8.21	-18.80	-134.69	-3.95	-13.50	29.88	-131.77	-4.36	8.93	-16.91
F	T-I	W	-108.61	-3.40	8.36	-22.69	-137.98	-4.29	-13.19	35.82	-136.80	-5.05	8.45	-20.97

Notes: 1) S = single span; T-E = triple exterior span; T-I = triple interior span.
2) B = bottom flange; T = top flange; W = web.

Conclusions and future work

Strength and behavior of corrugated steel decks of types B and F subjected to concentrated loads were studied on FE models. The developed non-linear FE models were validated against available test data. The following parameters were varied in the study: deck gage, span length, span condition, concentrated load locations along and across the deck span. The observed deck behavior under concentrated loads, as well as the effects of the studied parameters on the effective transverse distribution widths governed by the deck strength and stiffness, was presented and discussed. Design equations for predicting the effective distribution width for the studied deck profiles were presented.
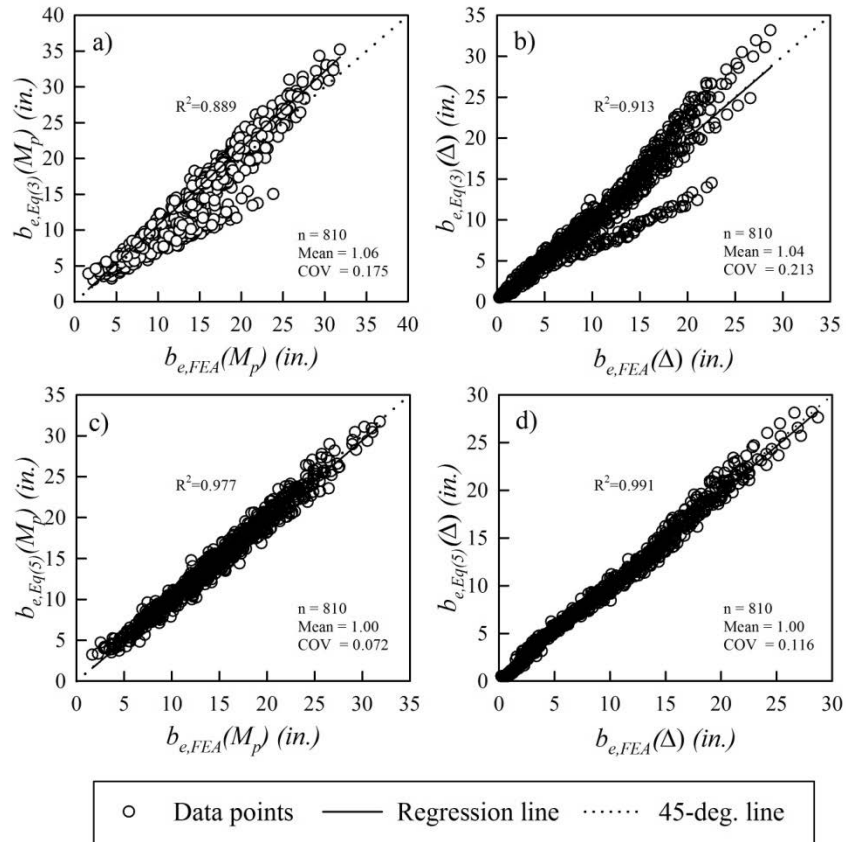
Fig. 6. Comparisons of the effective distribution widths obtained from FE simulations and calculated using developed equations: a) and b) Eq.(3) strength- and stiffness-controlled, respectively; c) and d) Eq.(5) strength- and stiffness-controlled, respectively

A numerical parametric study on the strength and behavior of different deck types, including deep deck and dovetail-shaped deck profiles, subjected to concentrated loads is currently underway. The developed design equations will be extended to other studied deck profiles. An attempt will be made to simplify and generalize the developed equations. An equivalent orthotropic shell model of corrugated steel deck is planned to be developed to allow engineers to model corrugated steel deck subjected to concentrated loads in general purpose structural analysis software available to practicing engineers.

Acknowledgements

References

Bahr, E. S. (2006). Transverse load distribution for a concentrated load on steel deck with plywood overlay. *Master's Thesis*, the University of Missouri-Rolla, Rolla, MO, USA.

Camotim D. & Silvestre N. (2004). GBT-based analysis of the distortional postbuckling behavior of cold-formed steel z-section columns and beams. *Proceedings of the 4th International Conference on Thin-Walled Structures*, Loughborough, 243–250.

International Code Council Evaluation Services. (2015). ICC-ES AC379-2015. *Fastening Systems for Use with Re-entrant-type Steel Deck Panel Profiles*.

International Code Council Evaluation Services. (2017). ICC-ES ESR-3477. *Versa-Wedge® Steel Deck Hangers*.

Johansson, G. (1986). Single load on trapezoidal steel sheet. *IABSE Reports*, 49, 99-106.

Keerthan P. & Mahendran M. (2011). Numerical modeling of Lite Steel beams subject to shear. *Journal of Structural Engineering*, *137*(12), 1428-1439.

Schafer, B.W. & , Peköz T. (1998). Computational modeling of cold-formed steel: characterizing geometric imperfections and residual stresses. *Journal of Constructional Steel Research*, *47*, 193-210.

Šorf, M., & Jandera, M. (2017). Trapezoidal sheet hangers and concentrated or linear load distribution in profiled sheeting. *ce/papers*, *1*(2-3), 1563-1570.

Steel Deck Institute. (2017). ANSI/SDI C-2017. *Standard for Composite Steel Floor Deck Slabs*.

Steel Deck Institute. (2017). ANSI/SDI RD-2017. *Standard for Steel Roof Deck*.

Steel Deck Institute. (2012). SDI RDDM1, *Roof Deck Design Manual*, 1st Edition, Fox River Grove, IL.

Ventsel, E., & Krauthammer, T. (2001). *Thin Plates and Shells: Theory: Analysis, and Applications*. CRC press.

Appendix. – Notation

b_e	effective transverse distribution width;
$b_e(M_p)$	effective transverse distribution width governed by deck positive moment capacity;
$b_{e,Eq.(3)}(M_p)$, $b_{e,Eq.(5)}(M_p)$	effective transverse distribution width governed by deck positive moment capacity predicted by Eq. (3) and Eq. (5), respectively;
$b_{e,FEA}(M_p)$	effective transverse distribution width governed by deck positive moment capacity obtained from FE analysis;
$b_e(\Delta)$	effective transverse distribution width governed by deck deflection;
$b_{e,Eq.(3)}(\Delta)$, $b_{e,Eq.(5)}(\Delta)$	effective transverse distribution width governed by deck deflection predicted by Eq. (3) and Eq. (5), respectively;
$b_{e,FEA}(\Delta)$	effective transverse distribution width governed by deck deflection obtained from FE analysis;
b_{tf}	deck top flange width;
COV	coefficient of variation;
L	span length;
M_n	deck nominal moment capacity per one foot of width;
M_P	positive moment in deck due to P_{max};
M_w	positive moment in deck at the point load location due to the deck self-weight;
n	number of simulations;
P	concentrated load;
P_a	allowable concentrated load;
P_{FEA}	ultimate concentrated load obtained from FE analysis;
P_n	nominal (ultimate) concentrated load;
P_{max}	maximum concentrated load from FE analysis;
t	deck base steel thickness;
R^2	coefficient of determination;
x	coordinate of concentrated load along the deck span;
$\Delta_{FEA}(0.6P_{max})$	deck deflection at the point load location due to the point load of $0.6P_{max}$, obtained from FE analysis;
$\Delta_t(0.6P_{max})$	deck deflection at the point load location due to the point load of $0.6P_{max}$, obtained analytically for one foot wide deck strip;
Δ_w	theoretical deflection of one foot wide strip of deck at the point load location due to the deck self-weight.